In-the-Wild Interference Characterization and Modelling for Electro-Quasistatic-HBC With Miniaturized Wearables

David Yang, Parikha Mehrotra, *Student Member, IEEE*, Scott Weigand, and Shreyas Sen, *Senior Member, IEEE*

***Abstract*—The emergence of Human Body Communication (HBC) as an alternative to wireless body area networks (WBAN) has led to the development of small sized, energy efficient and more secure wearable and implantable devices forming a network in and around the body. Previous studies claim that though HBC is comparatively more secure than WBAN, nevertheless, the electromagnetic (EM) radiative nature of HBC in >10 MHz region makes the information susceptible to eavesdropping. Furthermore, interferences may be picked up by the body due to the human body antenna effect in the 40-400 MHz range. Alternatively, electro-quasistatic (EQS) mode of HBC forms an attractive way for covert data transmission in the sub 10 MHz region by allowing the signal to be contained within the body. However, there is a gap in the knowledge about the mechanism and sources of interference in this region (crucial in allowing for proper choice of data transmission band). In this paper, the interference coupling modality in the EQS region is explained along with its possible sources. Interferences seen by the wearable in the actual scenario is a non-trivial problem and a suitable measurement EQS HBC setup is designed to recreate it by employing a wearable sized measurement setup having a small ground plane. For the first time, a human biophysical interference pickup model is proposed and interference measurement results using a wearable device are presented up to 250 kHz in different environmental settings.**

***Index Terms*—Human body communication (HBC), biophysical circuit model, interference, wearable, electro-quasistatic (EQS), human body antenna.**

I. Introduction

THE advent of technological evolution has led to the development of miniaturized and small form-factor on-body internet connected devices [1]. This introduction of small-sized wireless body area network (WBAN) wearables, injectables, ingestibles and implantables [2] has transformed the fields of healthcare monitoring and secure data transmission, by enabling information exchange to biomedical sensors, smart watches, mobile phones and allowed remote and continuous patient monitoring and feedback. Typically, WBAN devices employ radio waves to wirelessly communicate information. However, being radiative in nature they not only require a high power for transmission as they attenuate in power density while propagating through space but also can be easily intercepted by malicious eavesdroppers and get access to private user information [3]. Thus, there is need for more energy efficient and secure data exchange techniques. Alternatively, human body having a high-water content, and acting as a lossy wire-like conductive channel for signal propagation can be utilized [3], [4], [5], [6], [7], [8]. EM mode of HBC (>10 MHz) has predominantly been used for the purpose of communication with the primary bottleneck being the interference picked up by the human body antenna effect in the 40M-400 MHz range [9]–[11]. To avert this, narrowband (NB) implementations (20-80 MHz carrier frequency) utilizing static frequency bands with tolerable interference or adaptively hopping between bands based on the measured channel quality have become popularized [12], [13]. NB HBC, couples the modulated narrowband EM signals to the human body using a coupler instead of radiating it with an antenna. This reduces the energy consumption of 10nJ/bit in conventional WBAN systems to 110 pJ/bit in NB HBC [3], [14]. Although, NB HBC is more energy efficient than WBAN, the EM nature of communication nevertheless radiates signal outside the body rendering it as not secure for data transmission. Electro-quasistatic (EQS) mode of signal transmission using HBC forms an attractive means for energy efficient and covert data exchange for sub 10 MHz frequencies [3] as it couples the signal through the conductive layers below the skin enabling containment of the signal and has been shown to exhibit energy efficiency up to 10 pJ/bit [5]. However, to ensure efficient communication via EQS HBC, it is essential to characterize and model the interferences present. This paper explores the mechanism and sources of interferences by performing in-the-wild measurements using a wearable sized measurement device to emulate the interference picked up by a real scenario EQS wearable receiver.

Manuscript received August 17, 2020; revised April 19, 2021; accepted May 10, 2021. Date of publication May 19, 2021; date of current version August 20, 2021. This work was supported in part by Eli Lilly through the Connected Health care initiative, Air Force Office of Scientific Research YIP Award under Grant FA9550-17-1-0450 and the National Science Foundation Career Award under Grant CCSS 1944602. *(Corresponding author: David Yang.)*

David Yang is with the School of Electrical and Computer Engineering, Purdue University, West Lafayette, IN 47907 USA (e-mail: yang996@purdue.edu).

Parikha Mehrotra and Shreyas Sen are with the School of Electrical and Computer Engineering, Purdue University, USA.

Scott Weigand is with the Eli Lilly and Company, USA.

Digital Object Identifier 10.1109/TBME.2021.3082078

This paper is divided into the following sections: Section I builds insight into using EQS HBC as an alternative to WBAN to achieve better energy efficiency and security, in Section II we discuss the motivation for analyzing the environmental interferences which may hamper EQS HBC as well as discuss the need for a wearable measurement device, Section III gives a brief inkling of the previous HBC works and how we circumvent their shortcomings. A novel biophysical model for the human-interference pickup is elucidated in Section IV followed by the design of a wearable sized interference measurement device using COTS components in Section V. Section VI highlights the important considerations while analyzing the interference measurement results to distinguish between actual environmental interferences and peaks from non-idealities, followed by wearable device's in-the-wild measurement results in Section VII and finally, the paper is concluded in Section VIII.

II. Motivation

To effectively utilize the human body as a communication channel in the EQS region, it is desirable to understand the existing interferences and their sources in this frequency band (<10 MHz). However, it is a non-trivial problem as there is gap in the knowledge about the mechanism of interference coupling and its sources in the EQS HBC region. Additionally, the optimal EQS HBC scenario entails wearable devices having high capacitive input impedance and floating ground planes, hence, to correctly determine the interference magnitude picked up by these devices, grounded equipment previously used in HBC studies such as oscilloscopes (OSC) and spectrum analyzers (SA) become ineffective.

A. Need for Understanding Interferences in the EQS Region

In previous studies, human body was characterized as a high pass channel having high loss at low frequencies making these frequencies unusable [4] and mostly focused on the EM mode for HBC (>10 MHz). However recently, using voltage mode signaling and high impedance capacitive termination at the receiver end, the human body channel has shown to provide flat-band loss at low frequencies (Fig. 1) [7], [15] with the primary bottleneck being the effect of interference picked up by the body [10]. Thus, knowing the mechanism and effects of interference in the sub 10 MHz frequencies is of great importance for effectively using EQS HBC for secure and energy efficient data exchange.

There have been studies conducted on the effects and mechanisms of interference picked up by the human body only in the EM HBC region [16], where the interference coupling mechanism is through the human body antenna effect. However, in the EQS region (at low frequencies ~100 kHz), the antenna size (in this case the human body) needs to be around 750 m to act as an efficient antenna. Active antenna designs are a possible alternative, however, tend to consume more power as they operate at higher frequencies than EQS-HBC transceivers. Alternatively, in EQS HBC mode, the interference picked up by the human body can be explained through capacitive coupling [17]. In this mode, the signal from a transmitter gets capacitively coupled to the surface of human body creating electric fields and the receiver picks up the displacement current. The return path can be modelled as a capacitance between the earth's and the wearable device's ground [18]. Large surface area radiating devices act as interference sources and get capacitively coupled to the skin with nearby radiating sources having more impact on the received interference signal as compared to those at a greater distance.

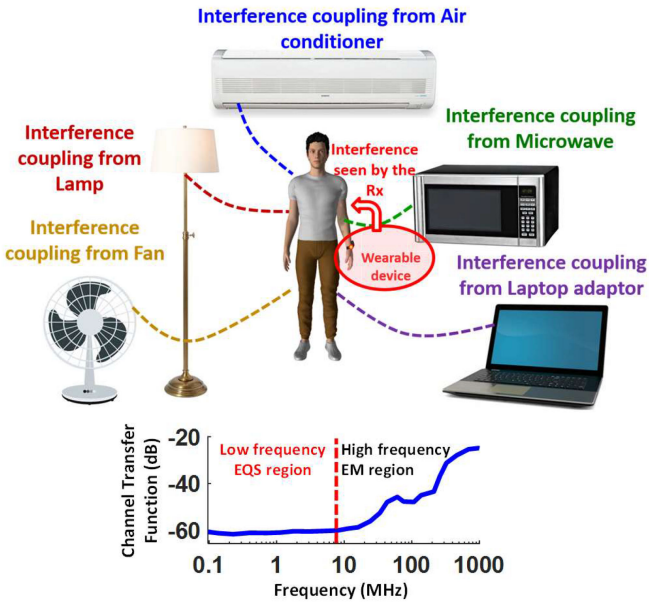

Fig. 1. Environmental interferences from electrical devices such as lamps, fans, and laptops couple to the human body posing a limitation on its effective usage as a communication channel in the EQS region. The plot shows the human body as a low loss broadband channel in the EQS region (sub 10 MHz).

B. Need for a Miniaturized Wearable Device for EQS HBC Interference Measurement

In EQS HBC, the device's transmitting/receiving electrodes are connected to the human body while the ground electrodes are left floating such that the human body forms the forward path of communication and the return path is formed by parasitic capacitances between the environment (earth ground) and the transmitting/receiving ground planes. The EQS HBC wearable devices are typically made with CMOS technology and have high capacitive input impedance with their ground planes floating. To effectively design EQS HBC transceivers, one must be mindful of the existing environmental interferences' magnitude and frequency. This received interference magnitude depends on the receiver's input impedance; hence it is important that the measuring equipment used must replicate the EQS receiver's input impedance. Furthermore, the return path capacitance for a floating ground wearable receiver is quite different from that of an earth grounded device, impacting the magnitude of interference observed. Both SA as well as OSC fail to satisfy these requirements. Fig. 2 intuitively compares the three scenarios for measuring the interference coupled to the body using a SA, OSC and a wearable (WR) measurement device. The SA is a small, resistive, 50 Ω terminated grounded device (having a large ground plane), while the OSC is a high input capacitive

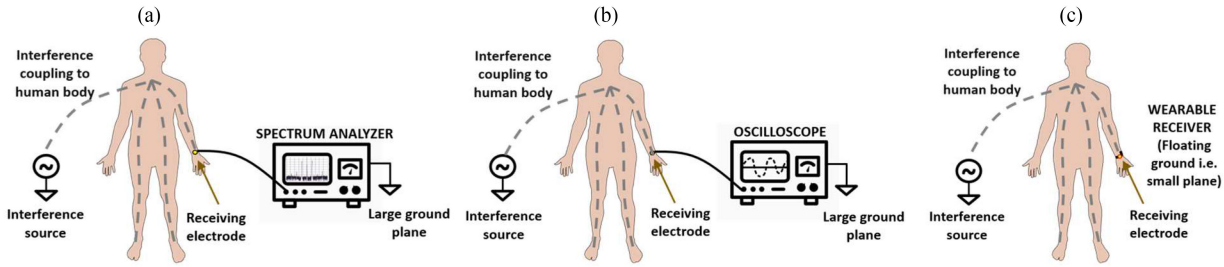

EQS HBC Features	SA	OSC	WR
High capacitive input impedance	✗	✓	✓
Small ground plane	✗	✗	✓
	Less interference is received even with a large ground plane.	More interference received compared to SA due to higher impedance termination.	Less interference received compared to OSC due to smaller ground plane.

Fig. 2. Choice of proper EQS HBC interference measurement setup which most closely replicates the interference picked up in the actual wearable scenario.

impedance terminated grounded device (also having a large ground plane). A small resistive termination implies a lower received signal than expected in an EQS HBC scenario due to the high pass response formed by the return path capacitance and the termination impedance of the spectrum analyzer [7]. While a large ground plane implies receiving a higher magnitude of interference voltage than expected. These two conflicting artifacts ultimately leads to pessimistic estimations of received interference due to the more prominent effect of the ground size. Hence, to closely match the magnitude of the interferences picked up by a wearable receiver, a miniaturized wearable interference measurement device is needed, both to match the input impedance of the actual wearable receiver as well as a floating ground condition (a small ground plane). Devices such as isolation transformers or commercially available battery powered spectrum analyzers do not provide sufficient ground isolation for accurate characterization of interferences [7].

TABLE I
COMPARISON SUMMARY BETWEEN PREVIOUS WORKS AND THIS PAPER

Parameter	[8]	[11]	Our work
Frequency Range	1-200MHz	30-120MHz	1-250kHz
Source of signal	Monopole antenna using battery powered RF source	Antenna using battery-powered signal generator	'In-The-Wild' Environmental interference
'In-The-Wild'	No	No	Yes
Antenna / Capacitor coupling	Antenna	Antenna	Capacitor
Measurement device	Spectrum analyzer	Spectrum analyzer	Miniaturized wearable
Input impedance of device	50Ω resistive impedance	50Ω resistive impedance	KΩ capacitive impedance
Grounded/ non-grounded	Grounded	Grounded	Non-grounded
Goal	Maximize HBC gain in EM HBC region using intentional signals	Determining SIR in EM HBC region using intentional signals	Determining unknown environmental interference in EQS HBC region

III. LITERATURE SURVEY

In previous studies [9], with the goal of determining the frequency bands with maximum HBC gain, the human subject was exposed to EM fields by intentionally applying a signal from a battery powered RF source generating 1-200 MHz (i.e., EM HBC region) signal through a 60 cm monopole antenna located 3m away as summarized in Table I. Human body and human arm resonances, i.e., maximum HBC gain frequency bands were estimated using an AC-powered SA (low input impedance grounded device) connected to an electrode touched by the human subject. In another study, human body antenna effect in the EM region of 30-120 MHz was observed using a 4-channel adaptive frequency hopping scheme [12]. The in-band interferences coupled to the body were measured on a SA (as seen earlier gives pessimistic interference measurement results) through a coaxial cable and a metal electrode attached to the left hand. The interferences through cordless phones and walkie-talkies were intentionally generated and coupled to the body and visualized. A 1.5Vpp signal at the transmitter side got attenuated to −50 dBm by the 1.8m body channel. The reduction in signal to interference ratio (SIR) in the FM band (80–110 MHz) was up to −20 dB, while the walkie talkie degraded the SIR to −22 dB. Both mentioned works studied the EM HBC behavior using intentional signals measured using earth grounded devices. Whereas, our focus in this paper is to examine the not so well known existing environmental interferences that could interfere with EQS HBC (sub 10 MHz) signals on getting capacitively coupled to the body. This is performed by using a miniaturized wearable measurement device as opposed to grounded devices used in previous studies that do not replicate actual wearable EQS HBC scenario.

IV. HUMAN BIOPHYSICAL MODEL FOR INTERFERENCE PICKUP

As mentioned earlier, the goal of this paper is to determine the existing environmental interferences that may couple to the body and degrade the performance of the EQS HBC wearable receiver. In this section, we will quantitatively distinguish between the

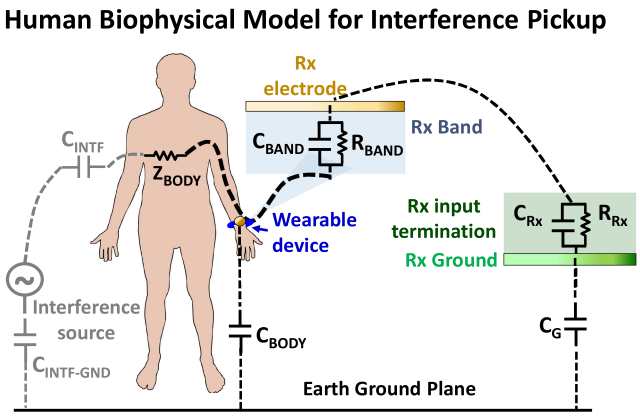

Fig. 3. Biophysical model of the human body capacitively coupled to a floating interference source.

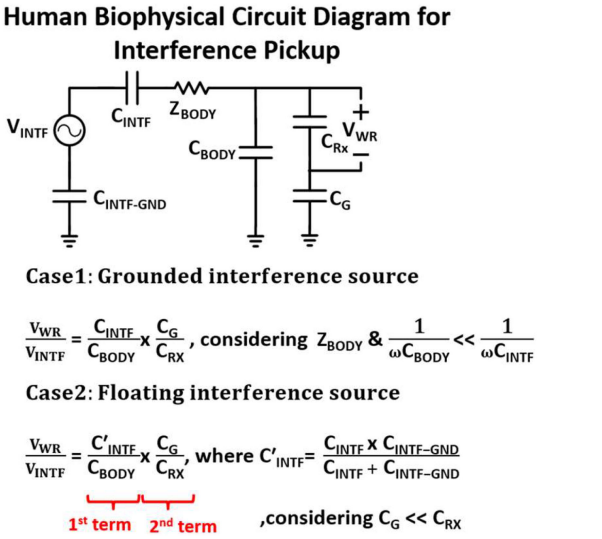

Fig. 4. Circuit diagram of the human body capacitively coupled to an interference source.

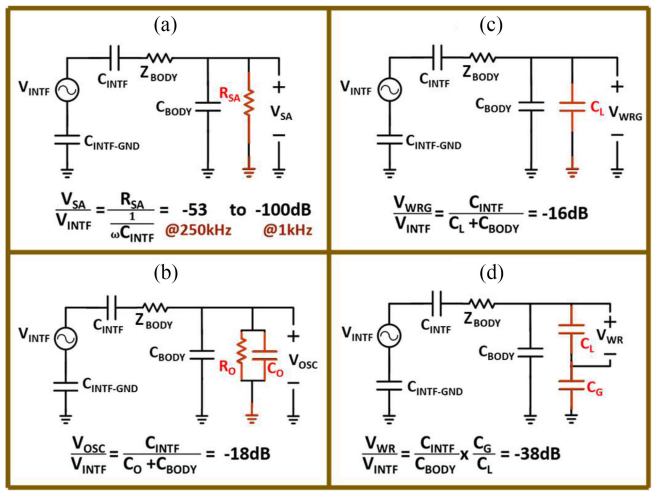

Fig. 5. Circuit diagram of the human body capacitively coupled to an interference source and measured using different devices (SA, OSC, WRG, WR). (a) R_x: SA. (b) R_x: OSC. (c) R_x: WRG. (d) R_x: WR.

three devices using circuit models; namely the SA, OSC and WR and determine how well they replicate the EQS HBC scenario. However, before we delve into the choice of equipment to be used for interference measurement, it is crucial to understand the passive models of the human body and of interference coupling to the human body as shown in Fig. 3. An interference source is essentially an EM radiation source, whose electric component couples to the body capacitively through C_{INTF}, assuming the body to be an equipotential surface. The interference source can have a floating ground and, in that case, introduces an interference source return path capacitance, $C_{INTF\text{-}GND}$. The coupled signal suffers impedance by the body tissue and skin as it flows through the body, denoted as Z_{BODY} ($\sim$1-10 kΩ consisting of tissue resistance in series with parallel combination of skin resistance and capacitance) [7], [19], [20]. This is received by the body worn wearable receiver through a tight skin contact with the receiver electrode (C_{BAND} ($\sim$200 pF), R_{BAND} ($\sim$100 Ω)) followed by the receiver's input termination (i.e., SA/OSC/WR) denoted by C_{RX} and R_{RX}. Return path capacitances exist between the body and earth ground at the receiving end (C_{BODY} of $\sim$150 pF) and between the receiver ground and earth ground (when the receiver has a floating ground, C_G is $\sim$1.2 pF, else can be considered a short circuit).

A simplified circuit diagram of human body interference pickup is shown in Fig. 4. Two possible cases are considered, namely, when the interference source is grounded and when the interference source is floating. In the latter, an extra $C_{INTF\text{-}GND}$ return path capacitance gets added in series with the C_{INTF}. V_{INTF} is the input interference voltage that gets coupled to the body and V_{WR} represents the voltage received by the wearable. The forward path impedance (Z_{BODY}) is neglected in this calculation, as Z_{BODY} is of the order of 1-10 kΩ, whereas the impedance provided by C_{INTF} is assumed greater than 100 kΩ, for sub-MHz frequencies. Furthermore, the return path capacitance (C_G) is an order of magnitude smaller than the load capacitance (C_{RX}). Using these approximations, we obtain the ratio of V_{WR} and V_{INTF} as a product of two terms as shown in Fig. 4. The first term shows how much interference gets coupled to the body and is a function of C_{INTF} and $C_{INTF\text{-}GND}$. Thus, the first term reduces with increase in distance between the body and the interference source as it reduces the capacitive coupling (C_{INTF}) between them. It is further reduced, when the interference sources are floating due to the incorporation of $C_{INTF\text{-}GND}$, reducing the numerator of the first term. The second term depicts the percentage of the coupled voltage picked up by the wearable and is a function of the wearable geometry due to its dependence on C_G [20]. Ultimately, C_{BODY} (height, weight, posture, placement of wearable, and mobility of the human subject) has relatively little bearing on the interference model as both the capacitances C_g and C_{INTF} will be higher impedance and dominate the amount of interference that should theoretically be coupled to the body.

Having developed an understanding of the biophysical model for interference pickup, we can modify it for different receiving equipment as shown in Fig. 5. With Spectrum Analyzer as the measurement device for picking up interference coupled to the body, the load offered by it is resistive and small in impedance (i.e., R_{SA} is 50Ω). Also, since it's plugged to the power supply ground, C_G is short circuited. This implies that most of the signal

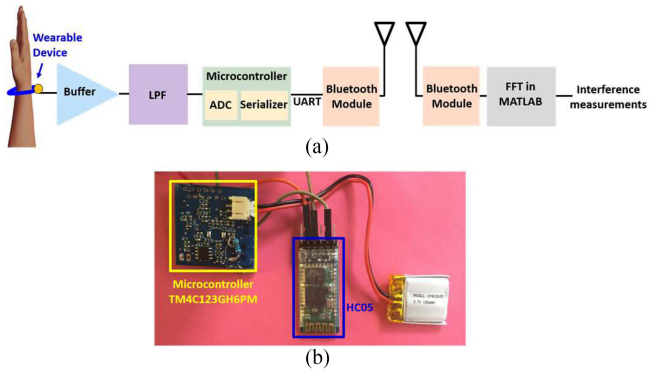

Fig. 6. (a) Block diagram of the wearable interference measurement setup. (b) Wearable setup using COTS components to acquire the interference data.

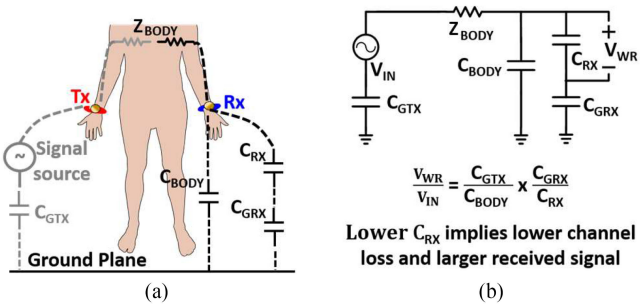

Fig. 7. (a) Human biophysical model for EQS HBC scenario. (b) A simplified circuit model explaining the choice for a high capacitive input impedance EQS HBC wearable receiver for minimizing channel loss.

is lost due to the high impedance of the body and the received interference signal is lower than what is expected in a wearable scenario. Assuming C_{INTF} to be 30 pF, the normalized received voltage at the SA (V_{SA}/V_{INTF}) has a frequency dependence and ranges from -53 to -100 dB in the 1-250 kHz EQS region (Fig. 5(a)). In case of OSC, the termination impedance is a parallel combination of C_O (80 pF) and R_O (1MΩ) [7]. Due to both its input impedance being high and being directly connected to the power ground, a higher interference voltage is received than would be expected in a wearable EQS scenario. Fig. 5(b) shows the normalized received voltage at the OSC to be (V_{OSC}/V_{INTF}) -18 dB. The input impedance of the wearable device measured using an LCR meter is (C_L) 20 pF. Connecting the wearable receiver to ground (referred as WRG in Fig. 5(c), where C_G gets short circuited), it behaves like the OSC, both having high capacitive input impedance and earthed ground. The normalized received voltage (V_{WRG}/V_{INTF} = -16 dB) is therefore very close to that of OSC. Finally, in Fig. 5d, the wearable ground is left floating, providing a C_G comparable to that expected in an EQS HBC receiver scenario and receives a normalized voltage of (V_{WR}/V_{INTF}) -38 dB. From this analysis, we can approximate the variation of received interference using different measuring instruments: SA receives ∼15 to 62 dB less voltage than expected in EQS scenario, while an OSC receives ∼22 dB more. This motivates the requirement for a miniaturized battery powered measurement device for interference measurement purposes as both the previously used devices, SA and OSC cannot be used to accurately determine the real scenario EQS HBC interference magnitude.

V. Design of Miniaturized Wearable Measurement Device

The interference signals get coupled to the body and are received by the wearable electrode. The study was approved by the Institute Review Board (IRB). The conceptual block diagram of this interference measurement setup along with the actual assembly using commercial off the shelf components (COTS) is shown in Fig. 6. The block diagram describes the measurement setup implementation in detail. The measurement setup (35 × 35 cm PCB) was custom-built for the purpose of this project – containing an analog front end of an op-amp buffer (AD823 circuit 1) and a non-inverting amplifier with a gain of 4 (AD823 circuit 2) followed by a simple anti-aliasing first order low pass RC lowpass filter, where the 3-dB roll off is set at 250 kHz. The output of the lowpass filter is connected to the on-chip SAR-ADC contained in the TI (TM4C123GH6PM) Arm Cortex-M4 Microcontroller. The ADC is configured for 500 kHz operation, the maximum possible reliable operation on this microcontroller platform. The board includes the low drop-out regulators (TPS73633DBVT) to supply the board from a lithium-ion battery (PRT-13854: 30 × 20 mm). Finally, the UART peripheral from the TM4C123GH6PM is used to communicate the signals off the board using an HC-05 UART/Bluetooth interface. This interface is paired with a laptop to log the data monitored from the wearable during measurements."

This interface is paired with a laptop to log the data monitored from the wearable during measurements. The output of the analog circuitry is both characterized using bench-top oscilloscope + spectrum analyzer as well as through an anechoic chamber as a control measurement as discussed in Section VI of the manuscript.

The need for high impedance termination in the EQS receiver is to achieve low channel loss through the body. Fig. 7(a) shows the EQS HBC scenario where data is sent through a wearable transmitter, suffers impedance by the body and is received by the body worn wearable receiver. In this case, return path capacitances exist between the body and earth ground (C_{BODY} of ∼150 pF) and between the wearable grounds and earth ground (C_{GTX}, C_{GRX} ∼1.2 pF). Fig. 7(b) shows the simplified circuit model of EQS HBC and it can be noted that to minimize channel loss through the body (or in other words, to increase the received voltage V_{WR}), the design choice is to minimize C_{RX} (as increasing C_{GRX} would imply increasing the wearable device's ground plane size [20]). This is achieved by placing a buffer at the wearable receiver's input which provides a C_{RX} ∼20 pF.

Calibration: The wearable measurement device is calibrated using the setup as shown in Fig. 8. A known signal is applied using an arbitrary waveform generator (AWG) and connected to the miniaturized wearable receiver's input electrode. The amplified signal at the ADC input is probed using an OSC and matched to the AWG applied signal's amplitude as seen in the post processed FFT spectrum. It is to be noted, that calibration is carried out with the wearable device's ground earthed (i.e., on WRG instead of WR). This is advisable when using strong

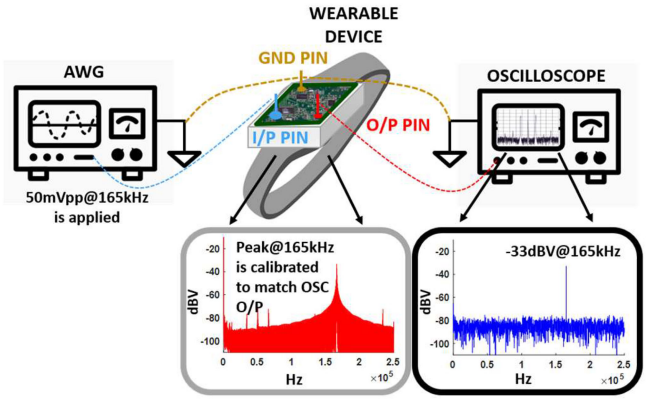

Fig. 8. Calibration setup: A signal is applied using an AWG and the received voltage at the output pin in the wearable is probed by an oscilloscope. This probed voltage value is matched to the wearable device's output value during post processing.

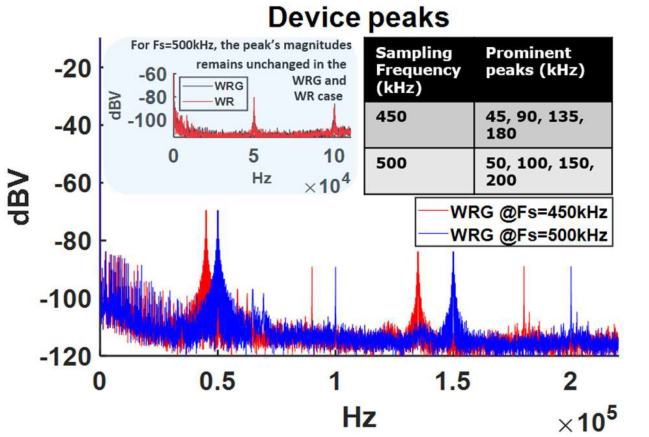

Fig. 9. Device peaks observed when sources of interference are turned off and sampling rates are varied (450k, 500 kHz). The subplot shows that the peak magnitude of the interferences (for Fs = 500 kHz) remains unchanged in the WRG and WR case.

grounded AWG and OSC, as keeping the wearable ground pin floating may create ambiguities coming from the return path (C_G) and affect the accuracy of calibration.

VI. Important Measurement Considerations

The goal of this paper is to identify the existing environmental interferences in the part of the EQS region that is sub-250 kHz, which may come from devices encountered in our everyday lives such as lights, fans, air conditioners etc. and may interfere with EQS-HBC. However, in order to correctly interpret the information obtained from the wearable measurement device, it is essential to understand the inherent nature of the wearable device first (i.e., to figure out if the device itself can add peaks to the spectrum) as well as the different phenomena and second order effects such as mixing and buffer nonlinearities which may create peaks in the frequency spectrum that may not be from actual environmental interferences. Also, developing an understanding of the noise floor (NF) and its dependencies is essential in characterizing the signal to noise ratio (SNR) and signal to interference ratio (SIR) for EQS HBC. Many of these challenges are unique to high impedance microcontroller-based measurement systems which have not been addressed in literature before but is the only correct way and needs a detailed discussion.

A. Inherent Device Peaks

To determine if the wearable measurement device itself caused any interference peaks, the EQS spectrum was observed in an anechoic chamber. On plotting the spectrum up to 250 kHz in Fig. 9 using grounded wearable device (WRG) with a sampling rate of 500 kHz (controlled by the ADC in the microcontroller using reference clock of 80 MHz), peaks @50 kHz, 100 kHz, 150 kHz and 200 kHz were observed. The only possible source that could create those peaks being in an anechoic chamber was the device itself. A second confirmation that the device was generating these peaks was achieved by changing the sampling rate to 450 kHz which shifted the peaks to 45 kHz, 90 kHz, 135 kHz and 180 kHz. If the peaks were from any other interference source, they would have retained their positions (i.e., we would have still seen peaks @50k, 100k, 150k and 200 kHz) even after changing the sampling rate. Another, indicator that these peaks come from the wearable device is that the peak magnitudes remain unchanged in the WRG and WR measurements, despite the additional factor from capacitive division due to the return path capacitance. Thus, it can be concluded that the wearable itself creates peaks in the spectrum (due to the microcontroller generated clock), depending on the sampling rate and are not to be confused with any interference source in further analysis.

B. Effect of Non-Ideal Anti-Aliasing Filter

An anti-aliasing low pass filter is added in the signal path of the wearable device such that any interference signal greater than the maximum frequency (= sampling rate/2 ~250 kHz) gets filtered out. However, due to the non-ideality of the second order LC filter employed due to size and filer order limitation, the rejection obtained beyond the cutoff frequency (>250 kHz) is moderate. Due to this, interference signals >250 kHz fold back and appear as peaks in the spectrum (following the equation; $f_a = f \pm kF_s$ where f_a is the aliased frequency, F_s is the sampling rate and k is an integer). This effect was verified by applying an intentional signal of 740 kHz from an AWG on WRG and was seen as an alias @240 kHz in Fig. 10.

C. Effect of Mixing of Interferences

Second order effects of mixing were observed while using the wearable device, where the interference signals got mixed with the device generated peaks (50 kHz, 100 kHz, 150 kHz, 200 kHz) to create new peaks. This was verified by applying a 240 kHz signal from an AWG on WRG as shown in Fig. 11. On mixing with the device's peaks- 100 kHz, and 200 kHz (with F_s= 500 kHz), generated new peaks @ 40 kHz, 60 kHz, 140 kHz and 160 kHz. The peaks at 60 kHz and 160 kHz were aliased versions of 340 kHz and 440 kHz as shown in Fig. 11's table, while the peaks generated from mixing between 240 kHz applied

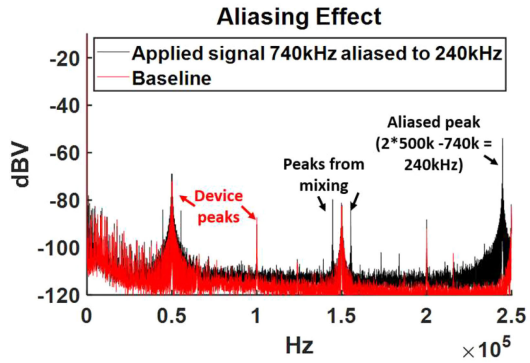

Fig. 10. On applying a signal (740 kHz) greater than the sampling rate (500 kHz), an alias is observed (@240 kHz) due to the non-ideality of the antialiasing filter (with cutoff @250 kHz).

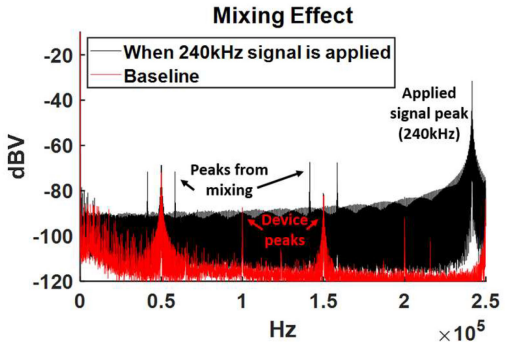

Peak 1 from applied signal (kHz)	Peak 2 from device when Fs=500ksps (kHz)	Mixed Peaks (Peak1±Peak2)	Comments
240	50	$290 \xrightarrow{aliased\ to} 210, 190$	Under NF
240	100	$340 \xrightarrow{aliased\ to} 160, 140$	Visible in Fig.
240	150	$390 \xrightarrow{aliased\ to} 110, 90$	Under NF
240	200	$440 \xrightarrow{aliased\ to} 60, 40$	Visible in Fig.

Fig. 11. The applied 240 kHz signal gets mixed with the device peaks (50k, 100k, 150k and 200 kHz) to generate new peaks @ 40k, 60k,140k and 160 kHz.

signal and the device peaks- 50 kHz and 150 kHz were smaller in magnitude and remained below the noise floor.

D. Effect of Buffer Non-Linearities

Another second order effect observed in the wearable measurement device's spectrum was from buffer nonlinearity creating new peaks at integer multiples of the interference signal. To illustrate this effect, a 44 kHz signal was applied from an AWG to WRG as shown in Fig. 12, and multiples of this signal were seen in the spectrum, i.e., @ 88 kHz (2^{nd} order) and 132 kHz (3^{rd} order). The higher order multiples reduced in amplitude and got buried under the noise floor. Thus, with respect to the baseline (where only device generated peaks are observed), on applying an intentional signal, all the additional peaks created can be explained through the combined effects of mixing and buffer nonidealities.

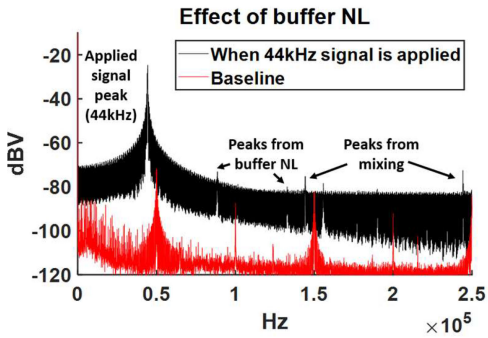

Peaks from Buffer NL (kHz)	Comments	Mixed Peaks (kHz)	Comments
44x2=88	Visible in Fig.	44±50=94, 6	Under NF
44x3=132	Visible in Fig.	44±100=144, 56	Visible in Fig.
44x4=176	Under NF	44±150=194, 106	Under NF
44x5=220	Under NF	44±200=244, 156	Visible in Fig.

Fig. 12. The applied 44 kHz signal creates new peaks due to buffer nonlinearities which are integer multiples of the applied signal.

E. Effects of Sample Size, FFT Size, Signal Strength and Windowing on the Noise Floor

The sensitivity of the wearable depends on the value of noise floor (NF), as any signal with a magnitude below it will not get detected, thus it is important to keep it to a minimum. It is possible to control the NF by choosing a proper duration (L) for which the ADC samples are recorded, and by choosing proper number of frequency samples (i.e., FFT points 'N') during FFT as shown in Fig. 13(a) & (b). From Fig. 13(a) it can be observed that on increasing the number of ADC digitized samples (i.e., feeding a longer length of samples to the post processing FFT algorithm), from L = 0.1M to 1M the NF reduces from −112 dBV to −120 dBV. Similarly, on increasing the number of frequency samples during FFT from N = 2^8 to 2^{16}, the NF reduces from −90 dBV to −110 dBV (Fig. 13(b)). Another factor which influences NF is spectral leakage, which occurs when the sample frequency is not an integral multiple of the FFT resolution, i.e., (Fs/N) and causes leakage of energy to other frequency bins as well instead of just the nearest frequency bin value [21]. Due to the unknown nature of the interferences being measured, it is not feasible to avert this effect. As a result, we encounter signal amplitude dependence of NF, as leakage of the signal to surrounding bins also increases with the increase in signal amplitude. Fig. 13(c) illustrates this by applying a known amplitude signal from the AWG (12.5mVpp, 25mVpp, 50mVpp and 100mVpp) and the NF is seen to increase by 20 dBV with a 4X increase in signal amplitude. Spectral leakage can be reduced by choosing an appropriate window function as shown in Fig. 13(d) which illustrates the effect of different windowing techniques (Hann, Blackman and Chebwin) on NF. Taking into consideration all the above factors, L of 10^5 samples and N of 2^{16} is chosen in our FFT algorithm for taking interference measurements with a suitable NF.

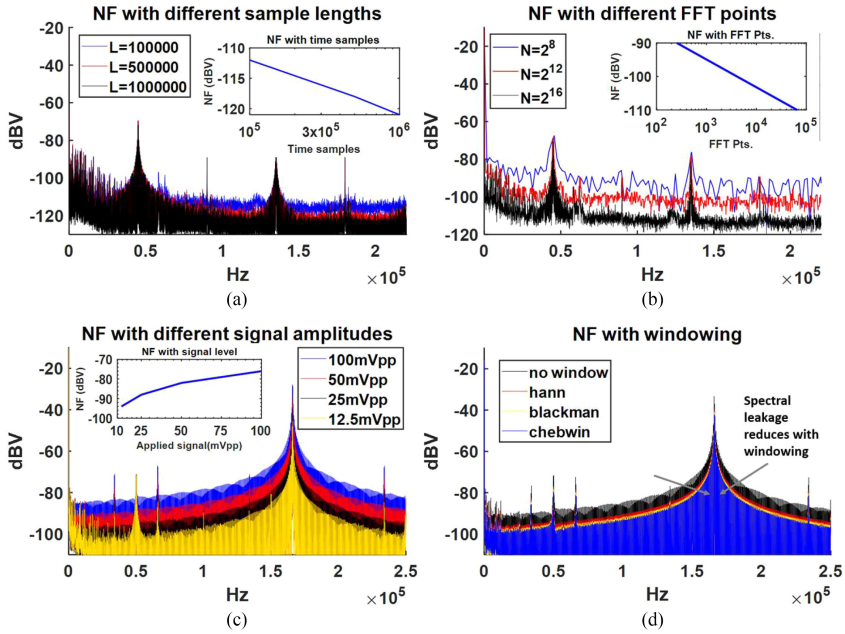

Fig. 13. Variation in value of noise floor (NF) with (a) different lengths of digitized ADC samples, (b) different number of FFT points/ bin size, (c) different applied signal amplitudes, and (d) different windows to reduce spectral leakage during FFT.

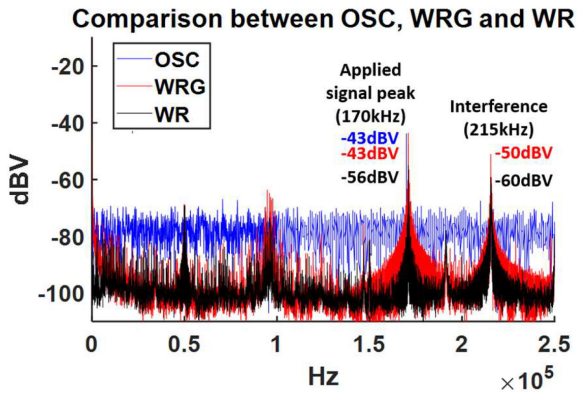

Fig. 14. A 170 kHz signal is applied from AWG and measured using OSC, WRG and WR.

F. Received Signal Magnitude in an Oscilloscope, Grounded Wearable Device and Non-Grounded Wearable Device

So far, we have applied AWG signals directly to the wearable receiver for verifying second order effects and to develop an understanding of the noise floor dependencies. To validate the theoretical models of Fig. 5 with different measuring devices, an AWG signal is applied on the body using a low impedance probe and is measured using an OSC, WRG and WR (Fig. 14). As predicted by the models in Fig. 5, the OSC and WRG received values are similar (−43 dBV @170 kHz), while the peak from WR is −13 dBV lower (−56 dBV @170 kHz). Apart from the intentional applied signal, we also observe an interference signal at 215 kHz in Fig. 14. The received signal amplitude in WRG is −50 dBV, while it is −60 dBV in WR, which is again a −10 dBV drop as expected.

G. Posture, Distance, and the Location of Measurement Device on Body

The experiments were conducted with the measurement wearable fixed onto the wrist of the subject through an electrode and have the subject extend their arm (with the measurement setup) perpendicular to their body full extended – to minimize coupling directly from an interference source to the device (not within the scope of this study). The source of interference is placed six feet in front of the human body.

VII. In-The-Wild Measurement Results

With this understanding about the different measurement devices available for interference measurement, we can now figure out the sources, the correct signal magnitudes and the frequencies of possible interferences which may exist in the EQS region (<250 kHz). For this purpose, we first collect baseline data at different locations; namely, a house bedroom, living room, an equipped electronic lab, and a commercial building hall (Fig. 15(a)). The house setting being a more flexible environment, the baseline is taken with all electronic appliances (such as lights, fans, refrigerators, stoves) plugged off, while the baseline in the lab is only with the lights turned off and all other appliances on (including computers, scopes, and signal generators). The baseline in the commercial building hall is without plugging out any appliance (and includes ceiling lights and a television). Measurements are carried out using an OSC, WRG and WR (where only the WR represents the actual wearable EQS HBC scenario). Once the baselines are acquired, the individual appliances can be turned on one at a time to observe their individual effect (i.e., whether they are responsible for any interference peaks in the EQS region) on the three measurement devices. The appliances tested for interference include –an air conditioner, a

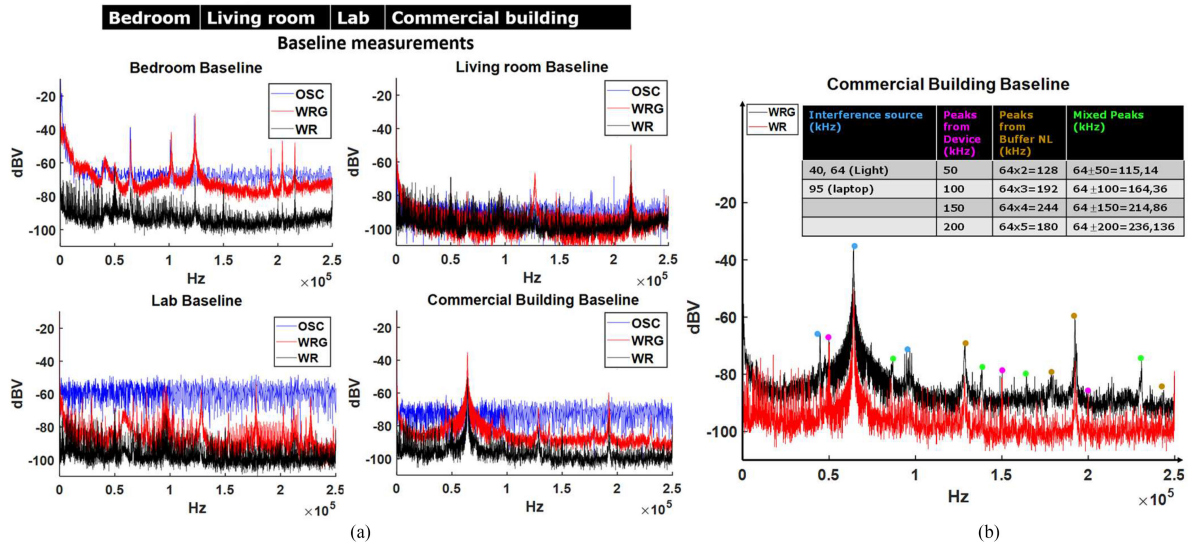

Fig. 15. (a) Measurement of baselines at different locations using OSC, WRG and WR. (b) Explanation of the peaks seen in the commercial building hall baseline.

fan, CFL light lamps, LED light lamps, fluorescent tubes, flush mounted CFL lights, a microwave, dimmable fluorescent tube lights, a stove, a refrigerator, a washing machine, and a laptop adaptor. On taking measurements after turning the bedroom air conditioner on (Fig. 16(a)) and comparing with the baseline bedroom measurement in Fig. 16(a), no additional peaks appear in the EQS spectrum observed using OSC, WRG or WR. All the peaks that we do observe in Fig. 17(a) (@64 kHz, 101 kHz, 122 kHz, 202 kHz and 214 kHz) were also present in baseline measurement with all appliances off (possibly coming from capacitive switching harmonics in supply) in Fig. 15(a), hence it can be concluded that there was no interference from the air conditioner. On performing similar analysis on other listed appliances, it was observed that the appliances that create peaks in the EQS region include CFL lights (Fig. 16(c), (e) & (h) @40-60 kHz), fluorescent tube lights (Fig. 16(f), (m) & (n) @40-60 kHz) and laptop adaptors (Fig. 16(o) @90-110 kHz), while all other appliances including LED lights (Fig. 16(d) & (i)), air conditioner (Fig. 16(a)), washing machine (Fig. 16(j)), stove (Fig. 16(k)), fan (Fig. 16(b)) and refrigerator (Fig. 16(l)) do not create any interference. To get a wider perspective of our in-the-wild measurements, an open field measurement was conducted (away from power lines and with no electronic appliances nearby) using WR as shown in Fig. 17. Peaks were observed @50 kHz and @150 kHz from the wearable device, and @95 kHz and @220 kHz from the laptop used for this measurement. The reason for appearance of peaks from devices is due to the power convertors (both DC/DC and AC/DC converters) employed, which are present in CFL and fluorescent lights, laptops, laptop adaptors and equipment with digital displays (in our case microwave). The switching frequencies employed by these converters appear as peaks in the spectrum. For instance, the switching frequency used by CFL and fluorescent drivers generally ranges from 40k-60 kHz, to achieve optimized performance as well as to avert human visible flicker. Laptop adaptors and phone chargers both house AC/DC converters, however, since laptop chargers work at higher voltage levels (12-25 V) compared to phone chargers (∼5V) they couple to the body more strongly and show up as interference peaks at around 90-110 kHz [22]. The peak shown from laptop adaptor is −60 dBV in Fig. 16(o), however, this measurement is the worst-case scenario as it is conducted on an old charger. Another important note is about interference from laptops itself, due to employment of laptop's Bluetooth in recording the measurement data, it is hard to circumvent its effect in the readings and is directly affected by the laptop's closeness to the subject's body wearing the wearable receiver. Laptops themselves have in-built DC/DC converters which result in a significant interference peak even without the adaptor @90-95 kHz. Though, it peaks @90-95 kHz, it is broadband in nature and may raise the NF over the entire EQS spectrum in worst cases. Hundreds of MHz to GHz operation devices such as mobile phones and Wi-Fi routers did not create interferences on the body despite being present. This is due to the small form factor of the device as well as low power supply voltages relative to laptop and other larger elements (both the C_{INTF} and C_g from Fig. 4 will be smaller, hence a higher impedance and lower interference characterized from the receiver perspective and also a lower V_{INTF}).

A possible solution to avert this broadband interference is through suitable channel encoding schemes to improve the SNR performance and reduce BER. Digital displays commonly present in microwaves, stoves and refrigerators also employ AC/DC converters to power the digital circuitry. To view the effect of digital displays, we use a microwave and its effect can be seen in Fig. 16(g). There is a slight increase in NF in the WRG measurement when microwave is turned on, however, no visible effect is observed in the WR measurement as the coupling from it is negligible due to smaller surface area (as compared to light from lamps and tube lights). Another interesting observation was made in the lab location having dimmable fluorescent tube lights (Fig. 16(m) & (n)). The lights showed two different frequencies at two different light settings, namely 40 kHz and 53 kHz attributed to its frequency-based feedback mechanism for changing the light intensity [23]. It is

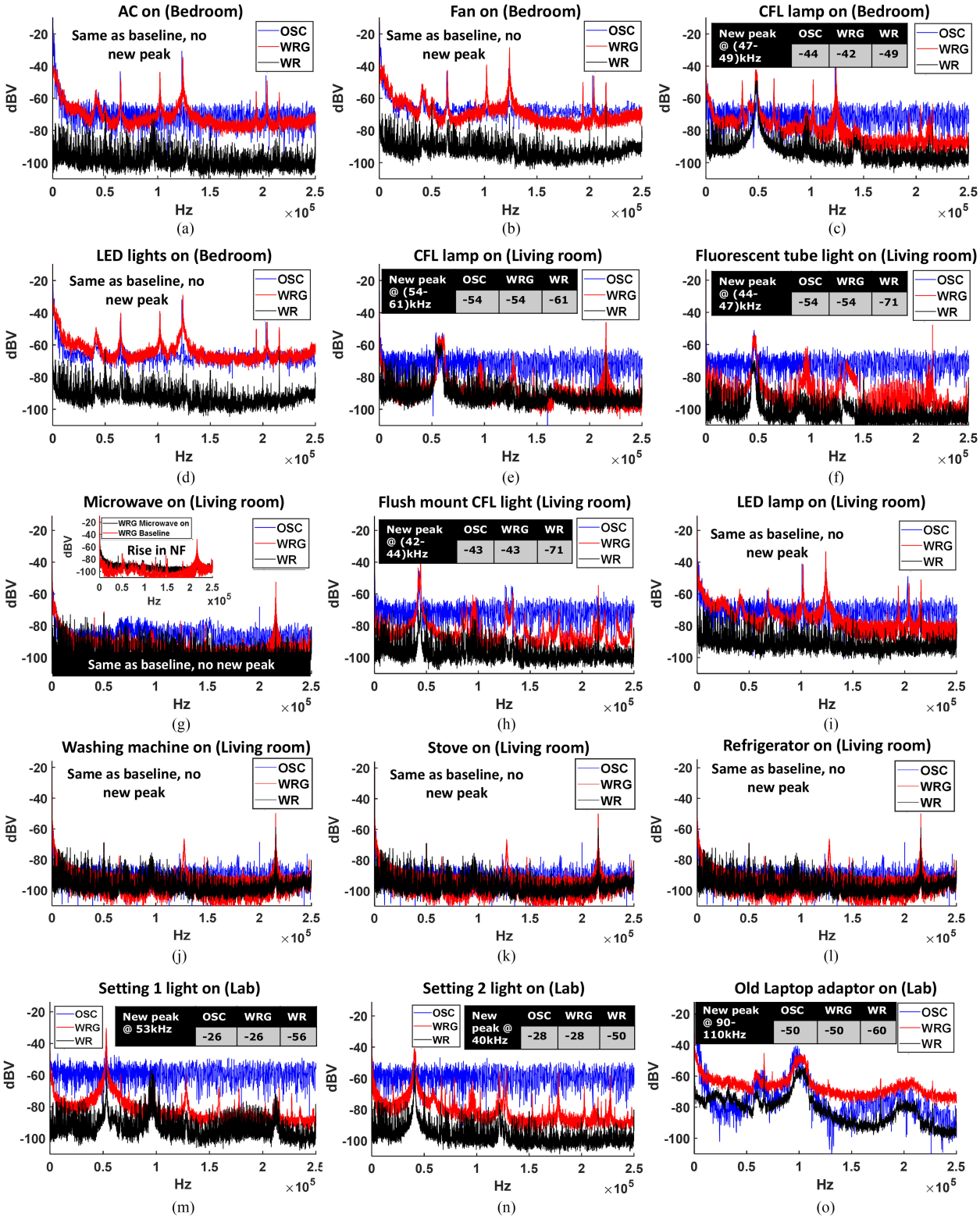

Fig. 16. Measurement of the effect of individual appliances in the EQS spectrum using OSC, WRG and WR at different locations.

to be noted that while CFLs and fluorescent lights cause interference peaks, LED lights do not. This is because LED drivers employ a much lower switching frequency of the order of 100's of Hz, hence not visible in the spectrum [24]. Also, additional peaks due to buffer nonlinearities show up while taking CFL and fluorescent light measurements (Fig. 16(c), (e), (f) & (h)) due to the high magnitude of interference peak recorded (∼50 dBV @44 kHz) giving rise to 2nd order peak @88 kHz, 3rd order peak @132 kHz and so on. All other appliances (stoves, refrigerators, fans, air conditioners) work on AC supply and show a peak at 60Hz (seen as a raised peak at DC in the measurements which is also due to the coupling of 60Hz main AC supply from house

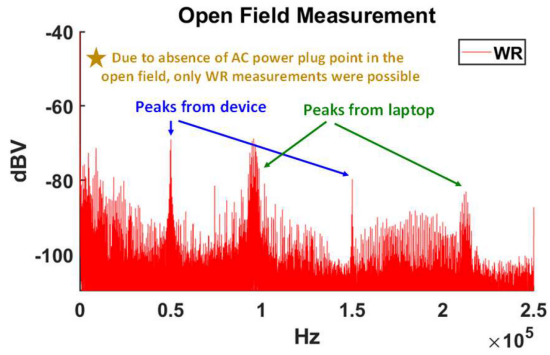

Fig. 17. Interference measurement in the EQS spectrum conducted in an open field using a wearable measurement device.

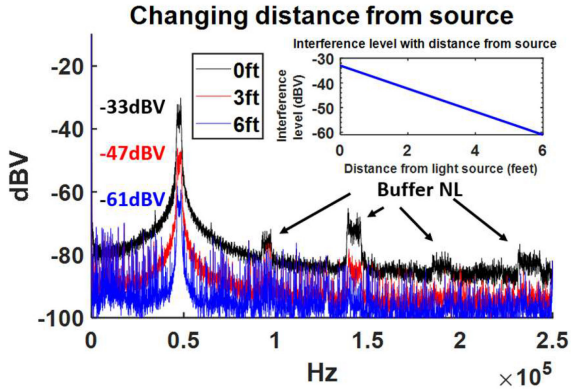

Fig. 18. Effect on received interfernce signal on WR on changing distance from source, or in other words varying $\mathbf{CINTF}$.

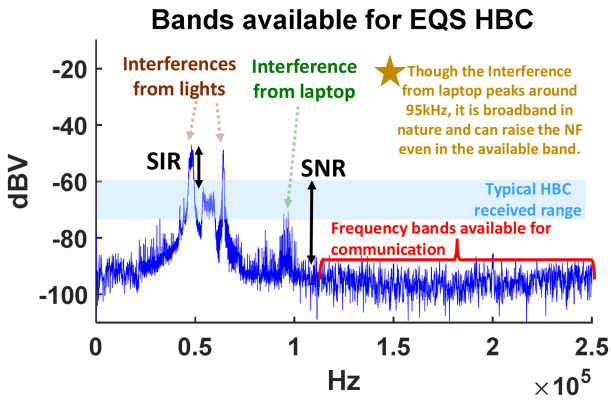

Fig. 19. Viewing all interferences from sources combined to determine the available bands for EQS HBC.

wiring to the body). In summary, we can say that the largest impediment in the EQS region are interferences from lights and laptops which must be accounted for while using EQS HBC.

With this understanding of the possible interference sources, we can now try to explain the peaks in the commercial building hall baseline (Fig. 15(b)). A significant peak is present around 64 kHz in WRG, which from our understanding can be attributed to the fluorescent lights present in the hall. Another observation is that the signal strength is quite high (~ -38 dBV) hence it is likely that second order products of mixing and buffer non-linearities will be present. On checking for peaks from mixing effect between the interference from fluorescent lights (64 kHz) and from the measurement device (50 kHz, 100 kHz, 150 kHz &200 kHz) as discussed in section VIC, peaks at 164 kHz ($= 64$ kHz $+ 100$ kHz) and 236 kHz ($= 64$ kHz $+ 200$ kHz $= 264$ kHz aliased to 236 kHz) were observed. Similarly, on checking for peaks from buffer nonlinearity at integral multiples of 64 kHz, peaks at 128 kHz (from 2nd order buffer nonlinearity $= 2 \times 64$ kHz), at 192 kHz (3rd order), at 244 kHz (4th order) and at 180 kHz (5th order) were observed. Additionally, an interference peak from laptop was observed @95 kHz. In summary, all the peaks in the commercial building hall can be explained to be coming from fluorescent lights and the laptop adaptor. This also reaffirms our statement that typically the major source of interference in any setting is from lights and must be taken care of during EQS HBC.

The effect of distance from interference source on the magnitude of received signal by the WR is shown in Fig. 18. This change in received signal with distance from source is due to change in C_{INTF} value. At about 2 inches from the CFL light bulb, the interference magnitude picked up by the WR is -33 dBV, -47 dBV at $\sim$3feet from source and -61 dBV at $\sim$6feet from source. Thus, it can be noted that the magnitude of interference picked up is strongly dependent on the closeness to the source. In other words, the reduction in distance between the source and body, increases C_{INTF} value which in turn enhances our received signal as explained in Fig. 4.

It is possible to avert the undesirable effects from device, mixing and buffer nonlinearities through improved receiver design. Under such circumstance, the EQS HBC band would be as shown in Fig. 19 which combines the observed peaks from our measurement results to better visualize the EQS spectrum and to choose the appropriate frequencies for communication, including the peaks from lights (40k-70 kHz) and from the laptop (90-100 kHz). It must be noted that the peaks present in the baselines (Fig. 15(a)) have not been included in Fig. 19 (e.g., @215 kHz), as they are location dependent. To this end, it may be useful for future EQS HBC devices to incorporate techniques that will take a decision on the choice of band real-time based on the detected interferences. However, coming back to the current in-the-wild measurements, Fig. 19 gives us an inkling about how the interferences as received by an actual EQS HBC receiver would be like. This is extremely useful in deciding for the proper choice of band for communication avoiding any potential interference regions. The typical EQS HBC received signal value ranges from ~ -60 to -75 dBV. The worst-case SIR of ~ -10 to -25 dB occurs below 100 kHz due to interference from light and is seen to improve beyond it, along with a sufficiently high SNR of $\sim$15 to 30 dB. Hence, the ideal choice for EQS HBC would be frequencies beyond 100 kHz where the possibility of any interference is less.

VIII. Conclusion

A proper choice of frequency band is needed for interference free EQS HBC as it will affect any data transmission through the body. The measurements conducted using oscilloscopes or spectrum/network analyzers as receiving equipment, does not accurately represent the actual wearable scenario in the EQS HBC frequency range (few MHz). This necessitates the use

of a battery-operated measurement device with a small ground plane and high capacitive input termination. Thus, a miniaturized wearable sized measurement device is designed which accurately recreates the actual wearable scenario and for the first time in-the-wild interference measurements using a wearable device are presented showing interferences from large surface area radiating devices such as power supply lines, switching circuitry in lights sources, digital displays, laptops and laptop adaptors which get capacitively coupled to the body and pose issues during communication. Furthermore, a human biophysical interference pickup model is proposed, and interference measurement results are analyzed allowing for a proper choice of band for interference-free operation beyond 100 kHz. The paper develops: 1) an Interference Coupling Bio-Physical Model that can be used to explain future measurements of interference on and the body during EQS communication 2) Interference data for real-world day to day use which will be useful for future EQS-HBC system designers as a reference and 3) a guidance towards available frequency bands for EQS-HBC. The model analyzes interferences for miniaturized wearables in the band of 0-250 kHz. Future work is necessary to characterize the region for the rest of the Electro Quasi-Static band (up to 10 MHz) for miniaturized transceiver designs operating at those frequencies in addition to other unwanted or spurious interference sources.

References

[1] S. Sen, "Invited - Context-aware energy-efficient communication for IoT sensor nodes," in *Proc. 53rd Annu. Des. Automat. Conf. - DAC '16*, Austin, TX, USA, 2016, pp. 1–6, doi: 10.1145/2897937.2905005.

[2] A. Ba *et al.*, "A 0.33 nJ/bit IEEE802.15.6/Proprietary MICS/ISM wireless transceiver with scalable data rate for medical implantable applications," *IEEE J. Biomed. Health Inform.*, vol. 19, no. 3, pp. 920–929, May 2015, doi: 10.1109/JBHI.2015.2414298.

[3] D. Das *et al.*, "Enabling covert body area network using electro-quasistatic human body communication," *Sci. Rep.*, vol. 9, no. 1, Dec. 2019, Art. no. 4160, doi: 10.1038/s41598-018-38303-x.

[4] Ž. Lucev, I. Krois, and M. Cifrek, "A capacitive intrabody communication channel from 100 kHz to 100 MHz," *IEEE Trans. Instrum. Meas.*, vol. 61, no. 12, pp. 3280–3289, Dec. 2012, doi: 10.1109/TIM.2012.2205491.

[5] S. Maity *et al.*, "BodyWire: A 6.3-pJ/b 30-Mb/s -30-dB SIR-Tolerant broadband interference-robust human body communication transceiver using time domain interference rejection," *IEEE J. Solid-State Circuits*, vol. 54, no. 10, 2892–2906, Oct. 2019, doi: 10.1109/JSSC.2019.2932852.

[6] S. Sen, "SocialHBC: Social networking and secure authentication using interference-robust human body communication," in *Proc. Int. Symp. Low Power Electron. Des. - ISLPED '16*, San Francisco, CA, USA, 2016, pp. 34–39, doi: 10.1145/2934583.2934609.

[7] S. Maity *et al.*, "Bio-physical modeling, characterization, and optimization of electro-quasistatic human body communication," *IEEE Trans. Biomed. Eng.*, vol. 66, no. 6, pp. 1791–1802, Jun. 2019, doi: 10.1109/TBME.2018.2879462.

[8] J. Bae *et al.*, "The signal transmission mechanism on the surface of human body for body channel communication," *IEEE Trans. Microw. Theory Tech.*, vol. 60, no. 3, pp. 582–593, Mar. 2012, doi: 10.1109/TMTT.2011.2178857.

[9] B. Kibret, A. K. Teshome, and D. T. H. Lai, "Human body as antenna and its effect on human body communications," *Prog. Electromagn. Res.*, vol. 148, pp. 193–207, 2014, doi: 10.2528/PIER14061207.

[10] B. Kibret, A. K. Teshome, and D. T. H. Lai, "Analysis of the human body as an antenna for wireless implant communication," *IEEE Trans. Antennas Propag.*, vol. 64, no. 4, pp. 1466–1476, Apr. 2016, doi: 10.1109/TAP.2016.2526070.

[11] B. Kibret, A. K. Teshome, and D. T. H. Lai, "Characterizing the human body as a monopole antenna," *IEEE Trans. Antennas Propag.*, vol. 63, no. 10, pp. 4384–4392, Oct. 2015, doi: 10.1109/TAP.2015.2456955.

[12] N. Cho *et al.*, "A 60 kb/s–10 Mb/s adaptive frequency hopping transceiver for interference-resilient body channel communication," *IEEE J. Solid-State Circuits*, vol. 44, no. 3, pp. 708–717, Mar. 2009, doi: 10.1109/JSSC.2008.2012328.

[13] S. Maity, D. Das, and S. Sen, "Adaptive interference rejection in human body communication using variable duty cycle integrating DDR receiver," in *Proc. Des., Automat. Test Eur. Conf. Exhib. (DATE)*, Lausanne, Switzerland, Mar. 2017, pp. 1763–1768, doi: 10.23919/DATE.2017.7927278.

[14] M. Nath *et al.*, "Inter-body coupling in electro-quasistatic human body communication: Theory and analysis of security and interference properties," *Sci. Rep.*, vol. 11, no. 1, Feb. 2021, Art. no. 1, doi: 10.1038/s41598-020-79788-9.

[15] S. Maity, K. Mojabe, and S. Sen, "Characterization of human body forward path loss and variability effects in voltage-mode HBC," *IEEE Microw. Wireless Compon. Lett.*, vol. 28, no. 3, pp. 266–268, Mar. 2018, doi: 10.1109/LMWC.2018.2800529.

[16] N. Cho *et al.*, "The human body characteristics as a signal transmission medium for intrabody communication," *IEEE Trans. Microw. Theory Tech.*, vol. 55, no. 5, pp. 1080–1086, May 2007, doi: 10.1109/TMTT.2007.895640.

[17] T. G. Zimmerman, "Personal area networks (PAN): Near-field intra-body communication," *IBM Syst. J.*, vol. 35, no. 3.4, pp. 609–617, 1996.

[18] M. A. Callejon *et al.*, "A comprehensive study into intrabody communication measurements," *IEEE Trans. Instrum. Meas.*, vol. 62, no. 9, pp. 2446–2455, Sep. 2013, doi: 10.1109/TIM.2013.2258766.

[19] J. Park, H. Garudadri, and P. P. Mercier, "Channel modeling of miniaturized battery-powered capacitive human body communication systems," *IEEE Trans. Biomed. Eng.*, vol. 64, no. 2, pp. 452–462, Feb. 2017, doi: 10.1109/TBME.2016.2560881.

[20] M. Nath, S. Maity, and S. Sen, "Towards understanding the return path capacitance in capacitive human body communication," *IEEE Trans. Circuits Syst. II Exp. Briefs*, vol. 67, no. 10, pp. 1879–1883, Oct. 2020, doi: 10.1109/TCSII.2019.2953682.

[21] A. Breitenbach, "Against spectral leakage," *Measurement*, vol. 25, no. 2, pp. 135–142, Mar. 1999, doi: 10.1016/S0263-2241(98)00074-8.

[22] S. Manuspiya *et al.*, "Laptop adaptor using a piezoelectric transformer -Drive circuit development-" p. 10.

[23] A. Tjokrorahardjo, "Simple triac dimmable compact fluorescent lamp ballast and light emitting diode driver," in *Proc. 25th Annu. IEEE Appl. Power Electron. Conf. Expo.*, Palm Springs, CA, USA, Feb. 2010, pp. 1352–1357, doi: 10.1109/APEC.2010.5433405.

[24] P. Fang, Y.-F. Liu, and P. C. Sen, "A flicker-free single-stage offline LED driver with high power factor," *IEEE J. Emerg. Sel. Top. Power Electron.*, vol. 3, no. 3, pp. 654–665, Sep. 2015, doi: 10.1109/JESTPE.2015.2436390.